



AFRL-RZ-WP-TP-2012-0137

**AC CURRENT DRIVEN DYNAMIC VORTEX STATE IN
YBa₂Cu₃O_{7-x} (POSTPRINT)**

A. Lucarelli, A. Frey, R. Yang, and G. Lüpke

The College of William and Mary

F. Grilli

Los Alamos National Laboratory

T. Haugan, G. Levin, and P. Barnes

**Mechanical Energy Conversion Branch
Energy/Power/Thermal Division**

FEBRUARY 2012

Approved for public release; distribution unlimited.

See additional restrictions described on inside pages

STINFO COPY

© 2007 Springer-Verlag

**AIR FORCE RESEARCH LABORATORY
PROPULSION DIRECTORATE
WRIGHT-PATTERSON AIR FORCE BASE, OH 45433-7251
AIR FORCE MATERIEL COMMAND
UNITED STATES AIR FORCE**

REPORT DOCUMENTATION PAGE					Form Approved OMB No. 0704-0188	
<p>The public reporting burden for this collection of information is estimated to average 1 hour per response, including the time for reviewing instructions, searching existing data sources, gathering and maintaining the data needed, and completing and reviewing the collection of information. Send comments regarding this burden estimate or any other aspect of this collection of information, including suggestions for reducing this burden, to Department of Defense, Washington Headquarters Services, Directorate for Information Operations and Reports (0704-0188), 1215 Jefferson Davis Highway, Suite 1204, Arlington, VA 22202-4302. Respondents should be aware that notwithstanding any other provision of law, no person shall be subject to any penalty for failing to comply with a collection of information if it does not display a currently valid OMB control number. PLEASE DO NOT RETURN YOUR FORM TO THE ABOVE ADDRESS.</p>						
1. REPORT DATE (DD-MM-YY) February 2012		2. REPORT TYPE Journal Article Postprint		3. DATES COVERED (From - To) 07 July 2005 – 07 July 2007		
4. TITLE AND SUBTITLE AC CURRENT DRIVEN DYNAMIC VORTEX STATE IN $\text{YBa}_2\text{Cu}_3\text{O}_{7-x}$ (POSTPRINT)				5a. CONTRACT NUMBER In-house		
				5b. GRANT NUMBER		
				5c. PROGRAM ELEMENT NUMBER 62203F		
6. AUTHOR(S) A. Lucarelli, A. Frey, R. Yang, and G. Lüpke (The College of William and Mary) F. Grilli (Los Alamos National Laboratory) T. Haugan, G. Levin, and P. Barnes (AFRL/RZPG)				5d. PROJECT NUMBER 3145		
				5e. TASK NUMBER 32		
				5f. WORK UNIT NUMBER 314532ZE		
7. PERFORMING ORGANIZATION NAME(S) AND ADDRESS(ES) The College of William and Mary Department of Applied Science Williamsburg, VA 23187-8795 ----- Los Alamos National Laboratory Superconductivity Technology Center Los Alamos, NM 87545				8. PERFORMING ORGANIZATION REPORT NUMBER AFRL-RZ-WP-TP-2012-0137		
9. SPONSORING/MONITORING AGENCY NAME(S) AND ADDRESS(ES) Air Force Research Laboratory Propulsion Directorate Wright-Patterson Air Force Base, OH 45433-7251 Air Force Materiel Command United States Air Force				10. SPONSORING/MONITORING AGENCY ACRONYM(S) AFRL/RZPG		
				11. SPONSORING/MONITORING AGENCY REPORT NUMBER(S) AFRL-RZ-WP-TP-2012-0137		
12. DISTRIBUTION/AVAILABILITY STATEMENT Approved for public release; distribution unlimited.						
13. SUPPLEMENTARY NOTES Journal article published in <i>Applied Physics A</i> , Vol. 88, 2007. © 2007 Springer-Verlag. The U.S. Government is joint author of the work and has the right to use, modify, reproduce, release, perform, display, or disclose the work. Work on this effort was completed in 2007. This paper has color content. PA Case Number: 88ABW-2007-0740; Clearance Date: 07 Jul 2007.						
14. ABSTRACT Time-resolved magneto-optical imaging measurements show that an ac current enables the vortex matter in $\text{YBa}_2\text{Cu}_3\text{O}_{7-x}$ thin films to reorganize into two coexisting steady states of driven vortex motion with different characteristics: a quasi-static disordered glassy state in the sample interior and a dynamic state of plastic motion near the edges. Finite element calculations consistent with the critical state model show good agreement with the measured field profiles in the quasi-static state but predict a larger hysteretic behavior in the dynamic state.						
15. SUBJECT TERMS magneto, coexisting, vortex, plastic, dynamic, calculations, disordered, hysteretic, model, films, edges						
16. SECURITY CLASSIFICATION OF:			17. LIMITATION OF ABSTRACT: SAR	18. NUMBER OF PAGES 10	19a. NAME OF RESPONSIBLE PERSON (Monitor) Timothy J. Haugan	
a. REPORT Unclassified	b. ABSTRACT Unclassified	c. THIS PAGE Unclassified			19b. TELEPHONE NUMBER (Include Area Code) N/A	

A. LUCARELLI^{1,✉}
A. FREY¹
R. YANG¹
G. LÜPKE¹
F. GRILLI²
T. HAUGAN³
G. LEVIN³
P. BARNES³

AC current driven dynamic vortex state in $\text{YBa}_2\text{Cu}_3\text{O}_{7-x}$

¹ Department of Applied Science, The College of William and Mary, Williamsburg, VA 23187-8795, USA

² Superconductivity Technology Center, Los Alamos National Laboratory, Los Alamos, NM 87545, USA

³ Air Force Research Laboratory, Wright-Patterson AFB, OH 45433-7919, USA

Received: 21 March 2007 / Accepted: 23 March 2007
Published online: 7 June 2007 • © Springer-Verlag 2007

ABSTRACT Time-resolved magneto-optical imaging measurements show that an ac current enables the vortex matter in $\text{YBa}_2\text{Cu}_3\text{O}_{7-x}$ thin films to reorganize into two coexisting steady states of driven vortex motion with different characteristics: a quasi-static disordered glassy state in the sample interior and a dynamic state of plastic motion near the edges. Finite-element calculations consistent with the critical state model show good agreement with the measured field profiles in the quasi-static state but predict a larger hysteretic behavior in the dynamic state.

PACS 74.25.Qt; 74.25.Ha; 74.25.Sv; 74.78.Bz

1 Introduction

Type-II and high-temperature superconductors (HTS) subjected to quasi-static changes of both an applied magnetic field and transport current have long been studied using different experimental methods. Hall sensor array [1], scanning Hall probe [2] and magneto-optical imaging [3] measurements have revealed interesting features of the magnetic vortex penetration in superconducting thin films, such as hysteretic, inhomogeneous and disordered states induced by the applied field and/or the transport current. These phenomena are generally understood in terms of the critical state theory [4, 5], which describes the behavior of the magnetic vortices in quasi-static changes of an applied magnetic field or a transport current. However, recent experiments have shown that the vortex mobility can be strongly affected by a dynamic magnetic field or ac current producing a number of novel effects, including: low frequency noise [6, 7], slow voltage oscillations [8], a history dependent dynamic response [9, 10] and a memory effect related to the direction, amplitude, duration, and frequency of the applied current [11]. Some of these effects in vortex physics have been ascribed to dynamic instabilities [1, 10–12] and transient [13, 14] or steady states of driven vortex motion created during the reordering induced by the applied current. Even more interesting is the dynamic in-

teraction of the vortex matter (VM) with a magnetic field and a current both applied at the same time, which is relevant to most HTS applications [15].

Here we present a detailed study of the effects of an ac current and a magnetic field on the dynamical vortex states in a $\text{YBa}_2\text{Cu}_3\text{O}_{7-x}$ (YBCO) thin film by using time-resolved magneto-optical (TRMO) imaging. Since TRMO imaging offers simultaneously high spatial and temporal resolution, it is suitable for accurate dynamic studies of magnetic flux distributions. We compare cross-sectional field and current profiles from our measurements with simulations using a recently developed method based on finite-element (FEM) calculations [16], which accounts for the thermally activated flux creep. Our results show that a quasi-static disordered glassy state develops in the sample interior in agreement with FEM simulations. A dynamic state of plastic motion forms near the edges, which exhibits negligible hysteretic behavior and reduced pinning strength. This effect is not revealed in the FEM calculations, which rely on the critical state model.

2 Experimental

Two-dimensional maps of the magnetic field perpendicular to the YBCO thin films are recorded with TRMO imaging. A detailed description of the setup can be found in [17]. Time resolution is achieved by stroboscopic imaging using a Q-switched frequency-doubled Nd:YLF laser (100-ns pulse length, 527-nm wavelength) with a pulse repetition frequency (PRF) tunable from single shot to 1200 Hz. The PRF of the laser is synchronized to the frequency of an ac current source. By shifting the phase, TRMO images can be taken at specific phase points over the whole period of the ac current with an accuracy $< 1 \mu\text{s}$. We use a polarizing microscope in a cross-polarized configuration, a digital camera with a resolution of 1344×1024 pixels, and a Bi-substituted ferrite garnet crystal as a magneto-optical (MO) indicator. In the TRMO measurements, a 4x-objective is selected to obtain a wide field of view of $3.4 \times 2.6 \text{ mm}^2$, which restricts the spatial resolution to a few microns.

The YBCO samples were grown by pulsed laser deposition on a LaAlO_3 or SrTiO_3 substrate with typical dimensions of $10 \text{ mm} \times 5 \text{ mm} \times 250 \text{ nm}$ [18]. The critical transition temperature (T_c) of the samples is 91 K, as determined

✉ Fax: 757-221-2050, E-mail: axluca@wm.edu

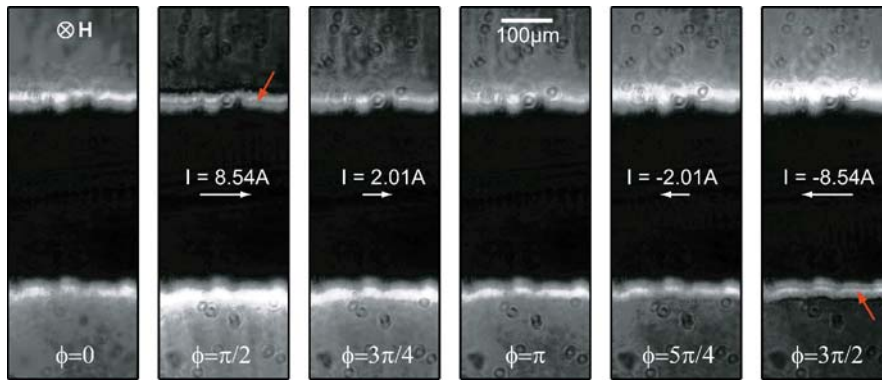


FIGURE 1 Time resolved magneto-optical images for different values of phase ϕ of the applied ac current. The white arrow in the center of the images indicates the current direction. The applied magnetic field is normal to the surface. The red arrows point towards the flux/anti-flux annihilation front

by ac susceptibility measurements. The samples are bridged using a photolithographic technique with a length of 6 mm and a cross-section $2w = 460 \mu\text{m}$ to reduce their critical current. A nanoparticulate dispersion provides strong pinning centers in the sample yielding a critical current density $J_c = 3.4 \times 10^6 \text{ A/cm}^2$ at 77 K.

In the TRMO experiment, the sample is cooled down to $T = 24 \text{ K}$ in a zero magnetic field. Upon reaching the temperature, a magnetic field $B_a = 10 \text{ mT}$ is applied perpendicular to the sample surface. An ac current $I(t) = I_0 \sin(2\pi ft)$ with $I_0 = 8.54 \text{ A}$ and $f = 1 \text{ kHz}$ is sent through the sample. At this temperature the applied current corresponds to about 32% of the critical current. We collect 25 TRMO images over the whole period of the ac current with a time step of $40 \mu\text{s}$.

3 Results and discussion

Figure 1 shows six images with focus on a small region of the bridge of about 10% of its length, which are taken at different phase points $\phi = 2\pi ft$ during the whole cycle. Bright areas in the images correspond to regions of high magnetic field near the edges of the sample. The dark area in the center of the images indicates the flux-free region. The uniformly gray region represents the intermediate magnetic field outside the sample. The penetration of the magnetic flux lines in the sample is cyclic, asymmetric and inhomogeneous, especially near the edges of the sample where the vortices form a pattern of narrow parallel bands, indicated by the red arrows in Fig. 1. The complex distribution of vortices specifically visible in the images at $\phi = \frac{\pi}{2}$ and $\phi = \frac{3\pi}{2}$ is a clear indication that the ac current rearranges the VM during the cycle.

Figure 2 shows cross-sectional magnetic field and current density profiles averaged over a sample length of about 1 mm for five selected phase points between $\phi = \frac{\pi}{2}$ and $\phi = \frac{3\pi}{2}$. Only the central part of the profiles ($|\frac{x}{w}| = |\bar{x}| \leq 2$) are shown in Fig. 2, but the measured profiles extend up to $|\bar{x}| = 5$ outside the sample. Current density profiles (Fig. 2b) are calculated from the magnetic field profiles by numerical inversion of the Biot–Savart law [19]. The gray shaded regions in Fig. 2 indicate the dynamic vortex state.

Figures 1 and 2 indicate clearly that the region of the highest magnetic field changes from one edge ($\bar{x} = 1$) to the other ($\bar{x} = -1$) according to the direction of the applied ac current and the induced self-field, since the external magnetic field is constant during the cycle. The regions where vortices and anti-vortices annihilate appear dark in the TRMO images. For

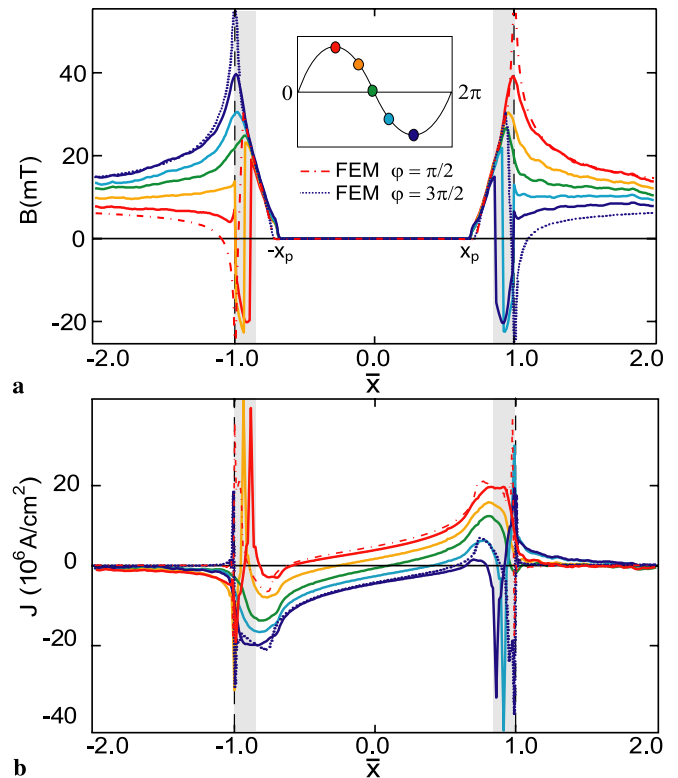


FIGURE 2 Field (a) and current density (b) profiles for different values of the phase. The phase points are indicated by the inset. The dotted lines show the sample edges

example in Fig. 1 at $\phi = \frac{\pi}{2}$ and $\phi = \frac{3\pi}{2}$, two such regions are visible as narrow dark lines (marked by red arrows). These two lines constitute the boundary of the negative flux region, and we accounted for them during the calibration of the images [19].

When the magnetic field $B_a(z) > H_{c1}$ is applied to the superconducting film, vortices penetrate the region ($|\bar{x}| \geq x_p$), where $x_p = 0.65$ ($x_p < w$) is the field dependent penetration depth as indicated in Fig. 2. This induces a shielding current density $J_{sc}(x, y)$ circulating in the sample that according to the critical state model reaches its maximum value J_c in the region ($|\bar{x}| \geq x_p$) where the flux penetrates. The Lorentz force, $F_L = (J \times B)$, created by the shielding current, is responsible for moving the vortices. The final equilibrium of the vortex phase in the HTS thin film is determined by the competition of F_L with four major interactions [20]:

- The thermal fluctuations (F_T) that favor a vortex liquid of lines or pancakes
- The vortex–vortex interaction (F_{vv}) that favors a perfect ordered vortex lattice
- The pinning (F_p) that instead favors an amorphous or glassy solid
- The coupling force (F_c) between layers that forms vortex lines from weakly interacting pancake vortices in adjacent layers

In HTS all these interactions have comparable energy scales so that the VM at equilibrium is rich in different phases. In YBCO thin films at low temperature and low field the pinning prevails over the other interactions, due to the strong anisotropy, the random distribution of surface barriers and defects. The VM at equilibrium is expected to be disordered and glassy; however, the application of a transport current density $J_{tr}(x, y)$ at a fixed temperature can rearrange the distribution of vortices.

J_{tr} increases the total current density J and hence F_L on one side of the sample while it decreases both on the other side. Additional flux penetrating from the edge shifts the flux penetration front further into the sample towards the center until it reaches a new equilibrium point where $\sum_i F_i = 0$. The critical state model predicts that the maximum current density region is extended uniformly to the new position of the flux penetration front and allows the calculation of the new current and field distributions [19]. However rapid variations of the field, as in the case of high-frequency alternating transport currents, can lead to a complete rearrangement of the VM and a more complicated behavior than predicted by the critical state model. Metastable, disordered vortex phases created by the transport current or a pulsed magnetic field have been previously observed in both type-II superconductors [1, 21] and HTS [11, 22]. In this case analytical solutions describing the time-evolution of the system become challenging to compute or even impossible to obtain especially if other effects, such as vortex phase transitions or flux instabilities, are included in the theoretical description.

In order to study the effects of the ac current on the VM we simulated the phase evolution of the field profiles by adopting a recently developed method based on FEM calculations. The model uses the direct magnetic field formulation without the use of vector or scalar potentials (common in conventional formulations) and relies on first-order edge finite elements [16]. The governing equations are Maxwell equations and the superconducting material is described by means of a non-linear E – J characteristic which takes into account the transition from the superconducting to normal state. In particular, the resistivity of the superconductor is expressed by

$$\varrho = \frac{E_c}{J_c} \left| \frac{J}{J_c} \right|^{n-1}, \quad (1)$$

where E_c is the critical electrical field, J_c is the critical current density and n is the power index defining the steepness of the transition. In our simulations, we used the values for the YBCO thin films used in the experiment at $T = 24$ K: $J_c = 2.2 \times 10^{11} \text{ Am}^{-2}$, $E_c = 10^{-4} \text{ Vm}^{-1}$ and $n = 19$. The non-linear dependence of the current and electric field expressed

in (1) is determined by the thermally activated flux creep [20]. The value of the exponent n is related to the ratio between the thermal energy and the flux pinning potential U_0 , which at the measured temperature corresponds to 40 meV. The field and the ac current simulation parameters are fixed during the simulation to experimental values: $B_a = 10 \text{ mT}$ for the magnetic field and $I_0 = 8.54 \text{ A}$ and $f = 1 \text{ kHz}$ for the current. In order to avoid transient effects, the tenth cycle of simulation has been considered for analysis. In Fig. 2 we compare the calculated profiles for two phase points $\varphi = \frac{\pi}{2}$ and $\varphi = \frac{3\pi}{2}$ to the measured data. The FEM simulations reproduce the flux penetration front, the shifting of the maxima with the phase and the asymptotic behavior outside the sample for all the measured phase points. Differences can be observed near the edges of the sample where the maximum peak of the measured profiles is reduced in intensity and the peak at the opposite edge is shifted further into the center of the sample.

Figure 3 shows the field (Fig. 3a) and current (Fig. 3b) distribution profiles measured and simulated with no net transport current flowing in the sample. The curves indicated by blue squares and red triangles are the profiles measured at $\varphi = 0$ and $\varphi = \pi$ when the voltage during the ac cycle is zero. At these phase points the electrons flow in response to the trapped magnetic flux lines and the measured current effectively represents a shielding current. These two current

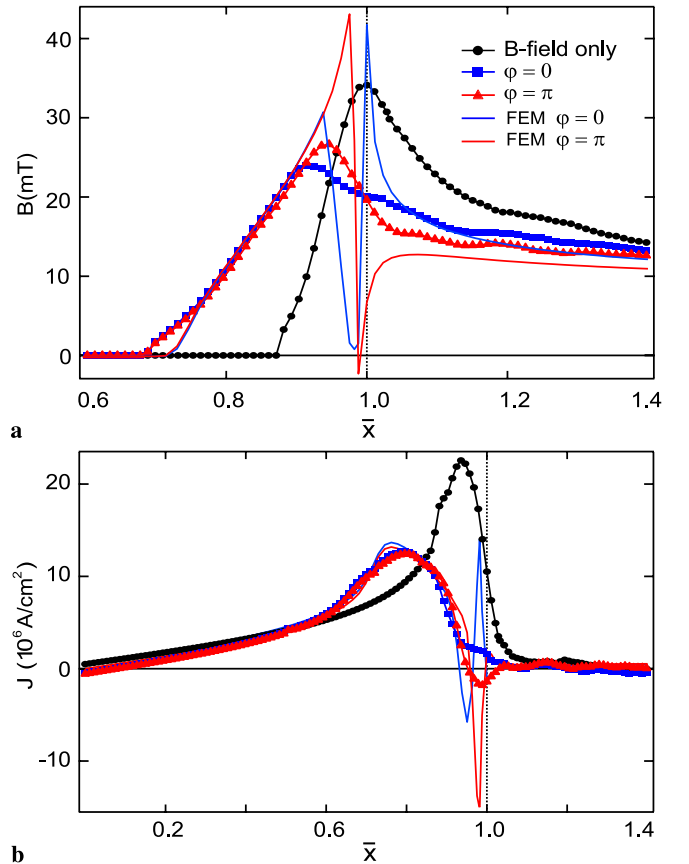


FIGURE 3 Current density profiles corresponding to the shielding current at $\varphi = 0$ and $\varphi = \pi$, compared to the shielding current density for the case of only an applied magnetic field of 10 mT without transport current. The dotted lines indicate the sample edges

profiles overlap fairly well over the whole sample width, with the exception of a small deviation in a region close to the edges. For comparison, we also show the shielding current distribution (black circle) induced by only the applied field $B_a = 10$ mT. The FEM simulations are also plotted in Fig. 3 as blue and red solid lines corresponding to $\varphi = 0$ and $\varphi = \pi$, respectively. The simulations at these phase points show a stronger hysteretic behavior than the measured profiles near the sample edge. The effect of the ac transport current is: (1) to reduce the peak shielding current, (2) to move the shielding current further inside the sample, and (3) to create a narrow gap at the edges where $J_{sc}(\varphi = 0, \pi)$ is strongly reduced and negligible hysteretic effects are observed.

The applied current softens the pinning, allowing the vortices to find more strongly pinned states inside the sample. The current that flows at the edges injects flux creating a transient disordered state. After a few cycles, subsequent to the flux injection the VM reorganizes in a steady state of driven vortex motion. The motion occurs in the presence of strong pinning centers that impede “smooth” entrance of the injected fluxions. At low temperatures there is a stationary phase at a low driving force and a dynamic phase above a critical de-pinning force. Since the penetration and exit of vortices requires a large F_L , due to the surface barriers much of the applied transport current flows at the edges in order to provide the necessary driving force [20, 23] and the rest phase is established in the center of the sample. The nature of the motion above the critical force can exhibit a wide variation [24]. In systems with random pinning, the motion is nearly always plastic at driving forces just above the critical force; that is, the vortices move at different velocities in different parts of the system [25]. Numerical simulations show that the plastic motion can take the form of rivers of moving vortices sliding between more stationary “river banks” [25].

4 Conclusion

In conclusion, we imaged for the first time the phase evolution of steady state vortex motion driven by an ac transport current. A quantitative study by TRMO imaging and FEM simulations reveals the formation and coexistence, during the ac cycle, of a quasi-static glassy state in the sample

interior and a disordered dynamic state near the edges of the sample.

ACKNOWLEDGEMENTS The work at CWM is partially supported by the DOE grant DEFG02-04ER46127. The work at LANL is supported by the US DOE Office of Electricity and Energy Assurance.

REFERENCES

- 1 Y. Paltiel, E. Zeldov, Y.N. Myasoedov, H. Shtrikman, S. Bhattacharya, M.J. Higgins, Z.L. Xiao, E.Y. Andrei, P.L. Gammel, D.J. Bishop, *Nature* **403**, 398 (2000)
- 2 R.B. Dinner, M.R. Beasley, K.A. Moler, *Rev. Sci. Instrum.* **76**, 103 702 (2005)
- 3 D. Denisov, D. Shantsev, Y.M. Galperin, E.-M. Choi, H.-S. Lee, S.-I. Lee, A. Bobyl, P.E. Goa, A.A.F. Olsen, T.H. Johansen, *Phys. Rev. Lett.* **97**, 077 002 (2006)
- 4 E. Zeldov, J.R. Clem, M. McElfresh, M. Darwin, *Phys. Rev. B* **49**, 9802 (1994)
- 5 E.H. Brandt, M. Indenbom, *Phys. Rev. B* **48**, 12 893 (1993)
- 6 G. D’Anna, P.L. Gammel, H. Safar, G.B. Alers, D.J. Bishop, *Phys. Rev. Lett.* **75**, 3521 (1995)
- 7 T. Tsuboi, T. Hanaguri, A. Maeda, *Phys. Rev. Lett.* **80**, 4550 (1998)
- 8 S.N. Gordeev, P.A.J. de Groot, M. Oussena, A.V. Volkov, S. Pinfold, R. Langan, R. Gagnon, L. Taillefer, *Nature* **385**, 324 (1997)
- 9 S. Kokkaliaris, P.A.J. de Groot, S.N. Gordeev, A.A. Zhukov, *Phys. Rev. Lett.* **82**, 5116 (1999)
- 10 G. Li, E.Y. Andrei, Z.L. Xiao, P. Shuk, M. Greenblatt, *Phys. Rev. Lett.* **96**, 0170091 (2006)
- 11 Z.L. Xiao, E.Y. Andrei, M.J. Higgins, *Phys. Rev. Lett.* **83**, 1664 (1999)
- 12 A. Pan, P. Esquinazi, *Eur. Phys. J. B* **17**, 405 (1999)
- 13 D. Giller, A. Shaulov, T. Tamegai, Y. Yeshurun, *Phys. Rev. Lett.* **84**, 3698 (2000)
- 14 B. Kalisky, A. Shaulov, Y. Yeshurun, *Phys. Rev. B* **68**, 012 502 (2003)
- 15 D. Larbalestier, A. Gurevich, D.M. Feldman, A. Polyanskii, *Nature* **414**, 368 (2001)
- 16 R. Brambilla, F. Grilli, L. Martini, *Supercond. Sci. Technol.* **20**, 16 (2007)
- 17 A. Lucarelli, G. Luepke, T.J. Haugan, G.A. Levin, P.N. Barnes, *Supercond. Sci. Technol.* **19**, 667 (2006)
- 18 T. Haugan, P.N. Barnes, I. Maartense, C.B. Cobb, E.J. Lee, M. Sumption, *J. Mater. Res.* **18**, 2618 (2003)
- 19 C. Jooss, J. Albrecht, H. Kuhn, S. Leonhardt, H. Kronmüller, *Rep. Prog. Phys.* **65**, 651 (2002)
- 20 R. Huebener, *Magnetic Flux Structures in Superconductors*, 2nd ed. (Springer, New York, 2001), p. 122 and p. 245
- 21 Y. Paltiel, D.T. Fuchs, E. Zeldov, Y.N. Myasoedov, H. Shtrikman, M.L. Rappaport, E.Y. Andrei, *Phys. Rev. B* **58**, R14 763 (1998)
- 22 D.T. Fuchs, E. Zeldov, M. Rappaport, T. Tamegai, S. Ooi, H. Shtrikman, *Nature* **391**, 373 (1998)
- 23 D.T. Fuchs, E. Zeldov, T. Tamegai, S. Ooi, M. Rappaport, H. Shtrikman, *Phys. Rev. Lett.* **80**, 4971 (1998)
- 24 A. Koshelev, V. Vinokur, *Phys. Rev. Lett.* **73**, 3580 (1994)
- 25 F. Nori, *Science* **271**, 1373 (1996)